



Design considerations for effective thermal management in mobile nanotweezers

Souvik Ghosh¹ · Ambarish Ghosh^{1,2}

Received: 6 October 2019 / Revised: 23 December 2019 / Accepted: 7 January 2020 / Published online: 14 January 2020
© Springer-Verlag GmbH Germany, part of Springer Nature 2020

Abstract

Controlled manipulation of nanoscale objects in fluids is relevant to both fundamental studies and technological advances in nanotechnology. While standard techniques of nanomanipulation, such as optical and plasmonic tweezers have limitations in simultaneous trapping and transport of nanoscale cargo, magnetically driven plasmonic nanorobots under optical illumination provide a promising solution. These so called mobile nanotweezers (MNT) use strongly localized electromagnetic field near plasmonic nanostructures to trap objects with high efficiency and can simultaneously be driven by magnetic fields to selectively trap, transport and release colloidal cargo. Upon illumination, apart from strong optical gradient forces due to local electric field enhancement, additional fluidic forces arise due to the heat generated by absorption of light. Here, we present a method to understand and engineer thermally induced fluidic forces in mobile nanotweezers. The temperature enhancement and associated thermofluidic forces are studied as a function of MNT geometry. We also discuss illumination at wavelengths slightly detuned from plasmon resonance frequency, which produces sufficient field enhancement with negligible generation of heat, and therefore much reduced thermophoretic and convective forces. This allowed us to engineer thermoplasmonic forces in MNTs for enhanced trapping performance and diverse applications.

Keywords Microrobots · Plasmonic tweezer · Optical nanomanipulation · Cargo transport · Plasmonic heating

1 Introduction

The ability to selectively trap and precisely manipulate arbitrary microscopic entities is one of the holy grails for small scale robotics. Manipulation of nanoscale cargo in fluidic environments is especially challenging due to the randomizing Brownian motion of colloidal particles, for which new techniques for trapping and transporting nanostructures need to be developed. In recent years several attempts have been made

towards developing artificial micro/nanorobots [1] to capture, transport and release cargo in fluidic environments [2–5]. Crucially, the microrobots can be driven quickly and with significantly good control overcoming random Brownian fluctuations. However, the method of cargo capture and release in most micromotors rely on chemical functionalization [6] and/or have magnetic elements [7] in both motor and the cargo, necessitating a high degree of chemical specificity in their interaction. A more general effort was made using magnetically actuated rods and doublets where the vortex flow associated with magnetic propulsion acts as fluidic tweezers to trap as well as transport colloidal cargoes in a non-invasive manner [2, 8–10]. However, fluidic micromanipulation becomes impractical as the size of the object reduces to sub-micron dimensions, which is also true for other conventional techniques such as optical tweezers [11] that suffers from diffraction limitation. Acoustic tweezers are also restricted by the diffraction limit, which implies the minimum size of the trapped particle will be comparable to or slightly less than the acoustic wavelength. For sub-micron colloids in water-like media, this necessitates very high acoustic frequencies [12]. In addition, the strength with which an object immersed in a fluid can be

Electronic supplementary material The online version of this article (<https://doi.org/10.1007/s12213-020-00123-6>) contains supplementary material, which is available to authorized users.

✉ Souvik Ghosh
souvikg@iisc.ac.in

✉ Ambarish Ghosh
ambarish@iisc.ac.in

¹ Centre for Nano Science and Engineering, Indian Institute of Science, Bangalore 560012, India

² Department of Physics, Indian Institute of Science, Bangalore 560012, India

trapped by an external force typically reduces with its volume, which becomes impractical as the size of the object reduces to sub-micron dimensions. Also, thermal fluctuations due to random collisions with the solvent molecules have strong randomizing effects as objects become smaller.

In this respect, strongly confined optical fields around plasmonic nanostructures under optical illumination can provide a promising alternative [13, 14]. Plasmonic tweezers can trap and manipulate objects as small as few nanometers with low optical power [15, 16]. However, the confining trapping potential is short ranged, typically within few tens of nanometers from the plasmonic nanoantenna, the can only trap particles in their vicinity. As a result, plasmonic manipulation is slow and their performance is limited by diffusion of colloids. Additionally, the plasmonic nanoantennas are fabricated on a nanopatterned substrate which defines the locations where colloids can be trapped. This in turn implies plasmonic tweezers are inefficient in transporting and arbitrary controlling the trapped objects unlike the fluidic tweezers.

Therefore, a common issue for both microrobots and plasmonic tweezers is the inability to trap and maneuver individual nano-objects throughout the fluidic volume. This long-standing limitation has been recently overcome by integrating plasmonics with magnetically driven nanoswimmers [17, 18], such as to develop a remotely steerable Mobile Nanotweezer (MNT) [19]. The resultant mobile nanotweezers can be magnetically driven close to any target object suspended in a liquid, which can subsequently be captured by shining appropriate optical illumination. The trapped object can be maneuvered to a different location and then released by reducing the illumination. This idea is shown schematically in Fig. 1a.

2 Motivation

The trapping mechanism in MNTs will always be aided by plasmonic gradient force whose origin is purely electromagnetic in nature. In addition, there may be contribution from heating induced by plasmon-enhanced optical absorption [20]. To explore both plasmonic and thermoplasmonics routes for colloidal manipulation, we have experimented with various MNT geometries. Here, we describe the thermoplasmonic-MNT (T-MNT) design, where small Ag islands are distributed throughout the surface of the helix as shown in Fig. 1b. Due to the effect of collective absorption from Ag nanoparticles, the T-MNTs show strong thermofluidic effects around them, which influenced the trapping process. We have studied the thermal [21] effects of T-MNTs on the surrounding liquid and investigated a few possibilities to control it. The paper is organised as follows. A brief introduction to plasmonic trapping mechanism and associated thermoplasmonics effects in MNTs are presented. Next, in the Methods section, we describe fabrication, actuation of the T-MNTs and present the experimental setup. Finally, in the

Results section, we demonstrate thermoplasmonic effects in the trapping process and various ways to control it.

2.1 Plasmonic nanomanipulation

When light is shined on to an object, it causes a displacement of the electron cloud, which results in a net dipole moment in the system. For sizes much smaller than the wavelength of incident light ($a \ll \lambda$), a particle can be considered a point dipole with a dipole moment $=\alpha E$, where the induced dipolar polarizability α determines the strength of interaction with the incident optical field. When such a dipole or collection of dipoles is exposed to an external electromagnetic field, it experiences a force given by,

$$\mathbf{F} = (\mathbf{p} \cdot \nabla)\mathbf{E} + \mathbf{p} \times \mathbf{B}$$

The first term originates from the inhomogeneous electric field and the second term is due to well-known Lorentz force. There is another contribution to the net force due to inhomogeneous magnetic field, which is negligibly small compared to the other two terms. For a given monochromatic electromagnetic wave with angular frequency ω and corresponding fields $\mathbf{E}(\mathbf{r}, t) = \mathbf{E}(\mathbf{r})e^{-i\omega t}$ and $\mathbf{B}(\mathbf{r}, t) = \mathbf{B}(\mathbf{r})e^{-i\omega t}$ the average mechanical force on the dipole is found to be

$$\langle \mathbf{F} \rangle = \frac{\alpha'}{2} \nabla \langle |\mathbf{E}(\mathbf{r})|^2 \rangle + \omega \alpha'' \langle \mathbf{E}(\mathbf{r}) \times \mathbf{B}(\mathbf{r}) \rangle$$

where α' and α'' are real and imaginary part of complex polarizability, respectively. The first term is called optical gradient force, which originates from field inhomogeneities and is proportional to the electric field intensity gradient. For a particle with a refractive index higher than the surrounding medium, the optical gradient force acts as an attraction which brings particles to the region of highest optical intensity. The second term corresponds to the scattering force, which is related to the imaginary part of the polarizability, is proportional to the local intensity and repulsive in nature.

2.2 Optothermal effects

In addition to the optical gradient force arising due to confined electromagnetic fields, there are also thermal-induced forces [22] present in the system which can play a crucial role in the trapping mechanism [23]. In any plasmonic system, resonant optical excitation induces both electromagnetic field enhancement and heat due to optical absorption [24, 25]. The generated heat increases the temperature of the plasmonic structure which initiates thermophoretic [26] and convective flow [27] in the surrounding fluid as described in Fig. 2.

Natural convection is a mechanism in which fluid flow is generated by local density changes in the fluid when subjected to heating. Due to the temperature increase that takes place

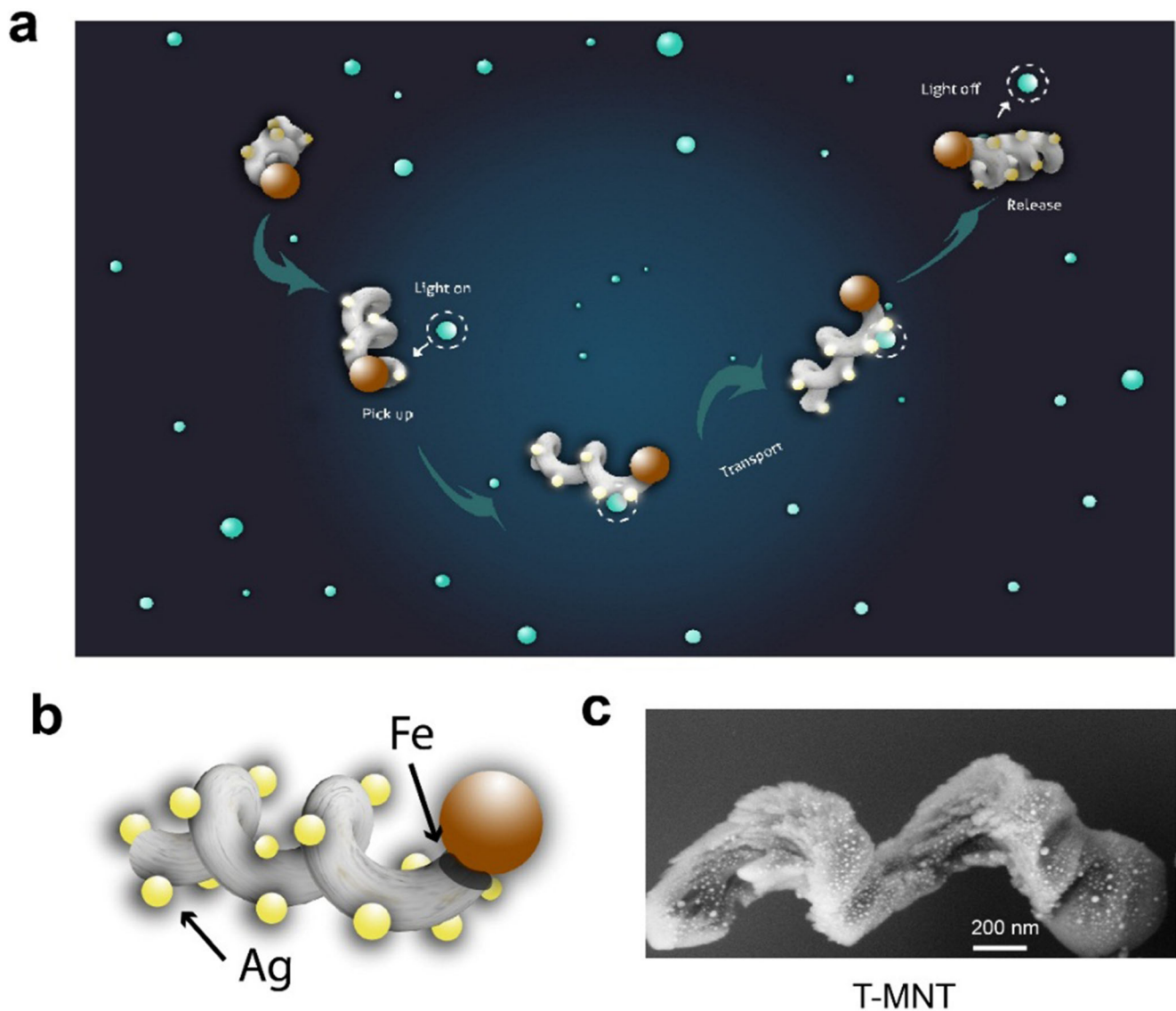


Fig. 1 Thermoplasmonic mobile nanotweezer. **a** Schematic of manipulation with a thermoplasmonic MNT (T-MNT). Trapping and releasing of the cargo can be controlled by turning the illumination on and off, while the MNT is maneuvered by external magnetic fields. **b** Schematic of T-MNT design, showing plasmonic (Ag) and magnetic (Fe)

particles. The helix is made of a dielectric (silica), and the head corresponds to a polystyrene bead on which the helix is grown using glancing angle deposition (GLAD). **c** SEM image of a T-MNT having plasmonic Ag particles all around its body.

within the fluid around a metallic nanostructure, the fluid density reduces resulting in upward motion due to buoyancy. The surrounding relatively cooler fluid then moves in, which is subsequently heated and moves upwards. This forms a convection current that can drive tracer particles suspended in a fluid towards the heated region [27]. Note convective flow can be strongly affected by geometry, especially height of the microfluidic device.

On the otherhand, thermophoresis is a phenomenon where particle motion in a fluid is induced by thermal gradients [22]. When a colloidal suspension is placed in a temperature gradient, the dispersed particles exhibits a steady drift velocity $v_T = -D_T \nabla T$, where D_T is thermophoretic mobility. In dilute

suspensions, the mass flow J can be written as $J = -D \nabla c - c S_T \nabla T$, where c is the particle concentration, D is Brownian diffusion coefficient and $S_T = \frac{D_T}{D}$ is called the Soret coefficient. Depending on the sign of S_T , the particles move either at the cold or the hot side. Like any other “phoretic” effects thermophoresis is fundamentally based on the inhomogeneity brought in by the temperature gradient in the thin layer that physically constitutes the interface between particle and solvent [26]. The interfacial tension gradients parallel to ∇T lead to anisotropic pressure distribution very close to the particle surface, so that the particle “pulls itself” in the direction of decreasing interfacial free energy. Various system parameters such as of the size of the colloid, solvent temperature, ionic

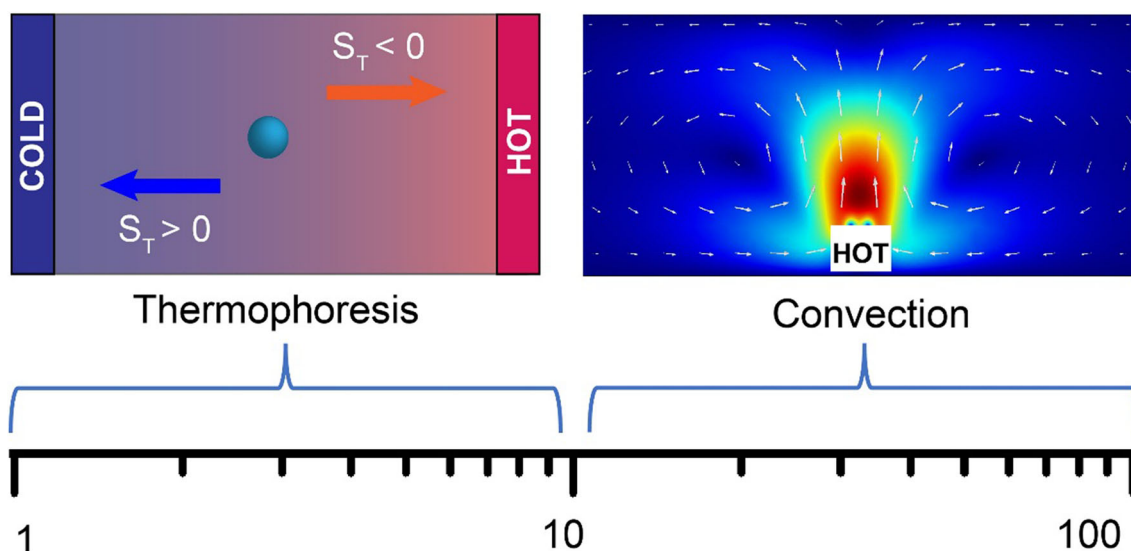


Fig. 2 Schematic illustration of thermal effects associated with plasmonic manipulation with typical length scales (in μm) shown below

concentration, surface chemistry etc., can affect the thermophoretic mobility and therefore the direction and magnitude of thermophoretic motion [28, 29].

Typically, these thermal forces have longer spatial ranges unlike plasmonic trapping force, which only extend upto a small fraction of the wavelength from the plasmonic particle. The thermophoretic forces exist along a strong temperature gradient ($\nabla T(z)$) present within a few micrometres from the heated object, whereas convection can be present at even longer distances. The nature of thermophoretic forces $F_{Th}(z) = -k_B T(z) S_T \nabla T(z)$ depends on the sign of the Soret coefficient (S_T) of the trapped object and therefore could either aid or hinder the trapping process. For example, a material with negative Soret coefficient such as silica experiences attractive force to the hot region, whereas a material with positive Soret coefficient such as polystyrene (PS) will get repelled. By carefully tailoring properties of the experimental system, it is possible to tune the sign of the Soret coefficient which enables trapping of various types of colloids as reported by Lin *et al* [30]. Depending on the details of the convective and thermophoretic forces, the opto-thermophoretic tweezers can trap nanoscale particles with less optical power than traditional plasmonic tweezers [31]. These findings have motivated us to investigate the various possibilities to tune the thermal effects and control the trapping behaviour in thermoplasmonic mobile nanotweezers (T-MNT).

3 Materials and methods

3.1 Fabrication of T-MNT

In this section, we will be discussing the wafer-scale fabrication of the magnetic nanoswimmers and the attachment of plasmonic nanostructures to it.

The fabrication of nanoswimmers starts with the formation of a seed layer on top of a flat substrate. We used a Langmuir-Blodgett Trough (Apex Instruments, Kolkata) to deposit a monolayer of colloidal beads (made of Polystyrene) on a substrate, which is depicted as a sphere in the schematic of Fig. 3. The resultant colloidal monolayer was fairly defect-free and was deposited throughout the entire Si wafer and could be directly used as the seed layer for GLAD. However, in order to avoid the chance of formation of connected networks [32] during the growth of microstructures, beads were often etched by air plasma ashing (Harrick Plasma cleaner) method.

The monolayer of PS beads acts as the template for the fabrication of the helical structures using GLAD [33], where the substrate was kept at an extreme angle (85°) with respect to the source of evaporated material. i.e. silica. During evaporation, the substrate was rotated slowly at one revolution per hour per μm of deposited silica, resulting in the formation of a helical nanostructure. Our fabrication method is highly scalable with yield of about 10 [8] helical nanostructures per cm^2 of substrate. The MNT fabrication steps are summarized in Fig. 3.

For magnetic actuation, the nanohelices are supposed to have permanent magnetic moments, for which we must integrate a ferromagnetic material (here Fe) to these microstructures. We have the flexibility to add the magnetic material at any desired spot of the helical nanostructure during its fabrication. To incorporate magnetic properties, prior to silica deposition, the seeded substrate was kept stationary and we deposited 5 nm of Ag, followed by 60 nm of Fe and another 5 nm of Ag. Here, Ag primarily served as an adhesion promoter between the ferromagnetic and the dielectric part.

In order to impart plasmonic properties, the silica helices grown on polystyrene beads were first taken out from

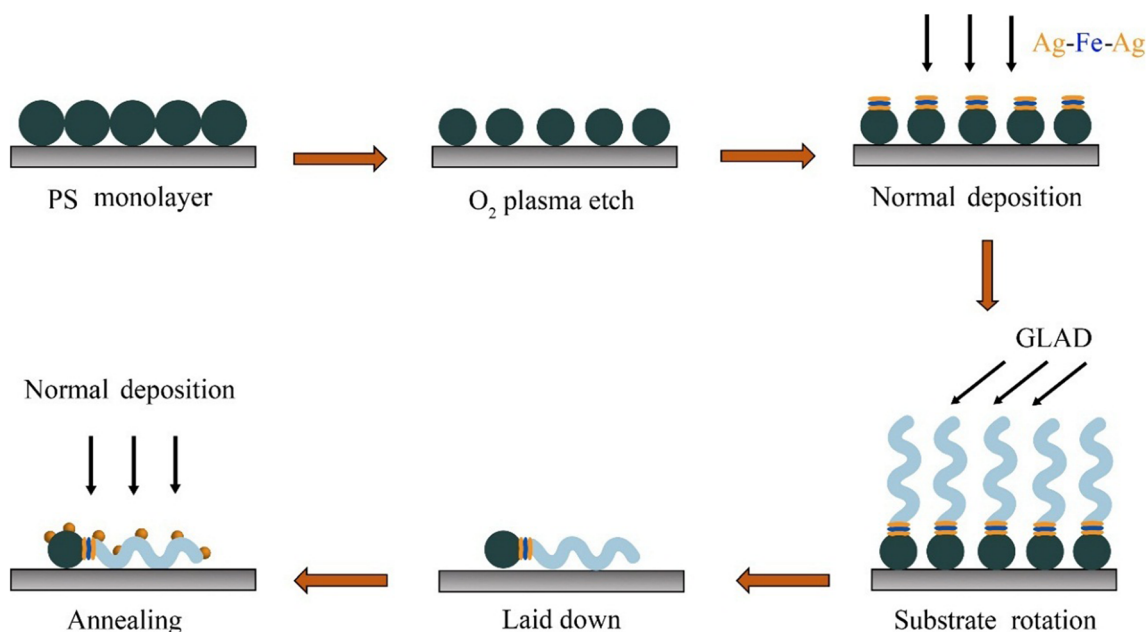


Fig. 3 Fabrication steps of T-MNT

wafer into water by sonication and the solution was then put onto a piranha cleaned Si wafer, so that the nanohelices were laid down. This is achieved by sonicating the standing helices in water and then spreading the solution on the Si wafer. On drying up the solution, the helices remain laid down on the wafer with random orientations. We then deposited a thin film (4 nm) of Ag on the MNT film followed by annealing at 300 °C for 1 min, such as to de-wet the film to form Ag nano-islands. This resulted in a large number of plasmonic nanoparticles all around the MNT, resulting in maximum absorption around wavelength 450 nm.

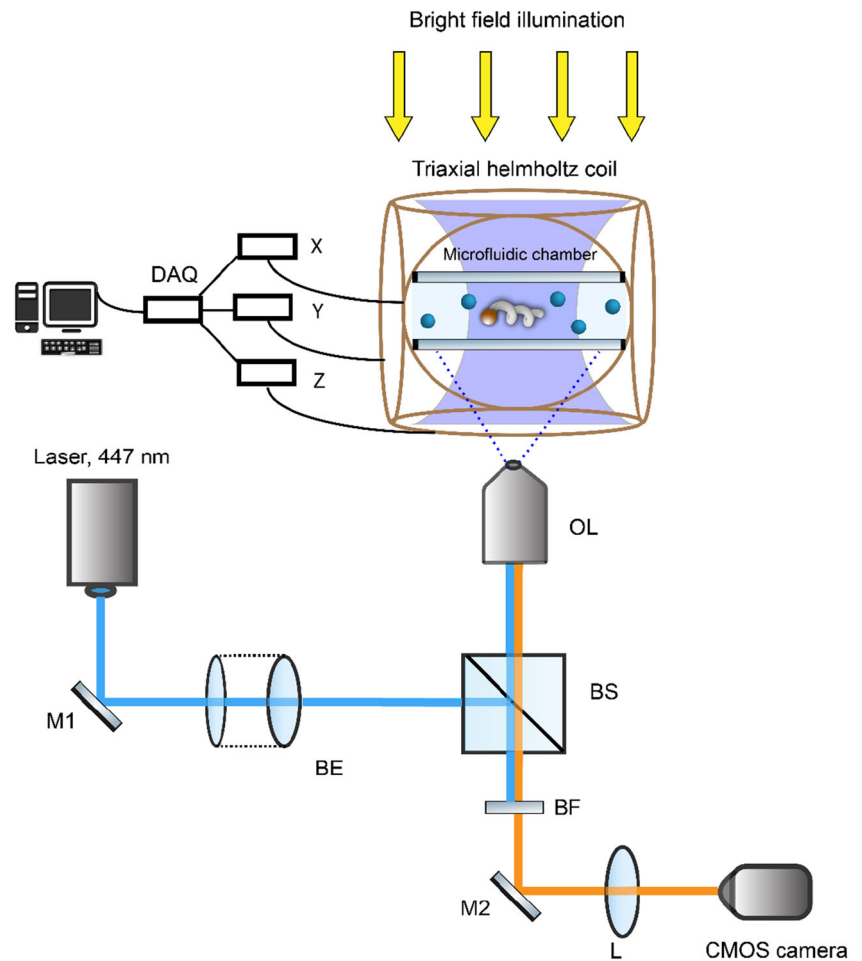
3.2 Experimental methodology

The experiments with the MNTs were mostly carried out by dispersing them in a homemade microfluidic cell. The substrate containing the MNTs was sonicated in deionized water for few seconds, such that the MNTs were detached from the wafer and got dispersed in fluid. Subsequently we prepared a fluidic suspension containing both MNTs and the colloidal particles (that were to be manipulated). A specific volume of the solution was then put in between two glass coverslips, depending on the desired thickness of the microfluidic cell. The MNTs typically stabilized close to the bottom wall of the chamber. All the experiments were carried out in deionized water at 25 °C. A defocused laser beam of variable power in mW range, was used to illuminate an approximate area between 100 and 1000 μm^2 . The experimental setup is shown in Fig. 4.

3.3 Actuation of T-MNT

The actuation principle of nanorobots was based on the inherent coupling of translational and rotational degrees of freedom in helical geometries. The rotating magnetic field \vec{B} applied a magnetic torque $\vec{\tau} = \vec{M} \times \vec{B}$ to the helix having a permanent magnetic moment \vec{M} . The applied \vec{B} field caused the permanent magnetic moment of the ferromagnetic MNT to rotate synchronously with the field, resulting in rotation and therefore translation (like a corkscrew) of the nanohelix along the direction governed by the sense of rotation of the applied field and handedness of the helix [34]. The direction of motion could be controlled in three dimensions by varying the plane and sense of the rotating field using a triaxial Helmholtz coil. The speed of the helix was proportional to the frequency (Ω_B) of the rotating magnetic field and the hydrodynamic pitch of the helix, provided the applied magnetic torque was higher than the drag from the surrounding fluid [35]. The magnetic setup consisted of three pairs of magnetic coils connected to three current amplifiers. These amplifiers generated sinusoidally varying currents (frequency Ω_B) which in turn were controlled by a voltage from a DAQ device. Considering X-Y plane to be the imaging plane of the MNT-bead system, the currents feeding into the X- and Y-coils were in-phase sinusoids generating magnetic fields $B_x = B_0 \cos(\Omega_B t) \cos(\alpha)$ and $B_y = B_0 \cos(\Omega_B t) \sin(\alpha)$. The current applied to the Z-coil pair was phase-shifted by $\pi/2$, generating a field of $B_z = B_0 \sin(\Omega_B t)$. This resulted in a net field of B_0 , which rotated in a plane perpendicular to the X-Y plane. The angle α was an experimental parameter that could be used to control the direction of the plane of the rotating field and therefore, the direction of the MNT in the X-Y plane.

Fig. 4 Experimental setup. Light from a 447 nm diode laser going through mirrors (M1 and M2), beam expander (BE), a beam splitter (BS), bandpass filter (BF) and lens (L) was transmitted through microscope objective illuminating a microfluidic chamber containing the MNTs and colloidal beads. It was also possible to couple the laser illumination from above, which is not shown here. The MNTs and the beads were imaged in a CMOS camera with bright field illumination from a Tungsten-Halogen lamp (marked in yellow). The tri-axial Helmholtz coil was built around the microfluidic chamber and was used to generate the magnetic fields.



4 Results

4.1 Temperature evolution in MNT system

To theoretically estimate the increased temperature at the surface of the MNTs, we find the absorbed thermal power density inside the metallic nanostructures, which can be written as,

$$Q(\mathbf{r}) = \frac{1}{2} \text{Re}[\mathbf{J}^*(\mathbf{r}) \cdot \mathbf{E}(\mathbf{r})]$$

where $\mathbf{J}(\mathbf{r})$ is complex amplitude of electronic current density inside Ag nanostructure, written as $\mathbf{J}(\mathbf{r}) = i\omega\mathbf{P}$ and $\mathbf{P}(\mathbf{r}) = \varepsilon(\omega)\mathbf{E}(\mathbf{r})$. In principle, an estimation of electric field $\mathbf{E}(\mathbf{r})$ can be obtained by solving the time-independent Helmholtz equation.

$$\nabla \times (\nabla \times \mathbf{E}) - k_0^2 \varepsilon(\omega) \mathbf{E} = 0$$

An exact calculation is computationally impractical considering the exact number of plasmonic particles and their arrangement around the helix vary across different MNTs. Instead, we could measure the average particle size and edge to edge distance among the particles which were found out to

be 30 nm and 5 nm respectively. The effective temperature increases due to collective heating of all nanoparticles can be estimated considering a periodic rectangular plasmonic array of finite size (length a , width b , periodicity $p = 35$ nm) using [36]

$$\Delta T = \frac{\rho_0}{4\pi\bar{k}} \int_{-a/2}^{a/2} \int_{-b/2}^{b/2} \frac{dx dy}{\sqrt{x^2 + y^2}}$$

where $\rho_0 = \frac{\bar{\sigma}_{\text{abs}} I}{p^2}$ is heat source density, \bar{k} is the average thermal conductivity of water ($0.6 \text{ W m}^{-1} \text{ K}^{-1}$) and glass ($1.3 \text{ W m}^{-1} \text{ K}^{-1}$), and I is incident light intensity. The temperature distribution in MNT and its outside is governed by

$$\nabla \cdot [\kappa \nabla T(\mathbf{r})] + \rho C_p \frac{dT}{dt} = Q \quad (\text{r})$$

where κ is thermal conductivity ($\text{W m}^{-1} \text{ K}^{-1}$), ρ is mass density (kg m^{-3}) and C_p is thermal heat capacity ($\text{J kg}^{-1} \text{ K}^{-1}$).

The resulting temperature can be assumed to be uniform over the metallic region due to large contrast of thermal diffusivity D in metal ($D \sim 10^{-4} \text{ m}^2/\text{s}$) and surrounding water medium ($D \sim 10^{-7} \text{ m}^2/\text{s}$). As $\left(\frac{\kappa}{\rho C_p}\right)_{\text{silver}} \gg \left(\frac{\kappa}{\rho C_p}\right)_{\text{water}}$, absorbed

heat diffuses faster inside metallic particle than surrounding dielectric environment and accumulates at the boundary before it diffuses into water. So, it can be assumed that the MNT-water interface maintains a uniform temperature under constant illumination. The timescale above which the uniform temperature approximation (UTA) is valid is given by.

$$\tau = \frac{R^2}{D}$$

where R is typical experimental length scale and D is thermal diffusivity ($\text{m}^2 \text{s}^{-1}$). As a consequence, for CW illumination we can consider steady-state heat equation to find out temperature distribution in water.

$$\nabla \cdot [\kappa \nabla T(\mathbf{r})] = Q \tag{r}$$

The simulated results are of similar magnitude as previous theoretical and experimental measurements, as reported by other groups in similar nanoplasmonic systems [36].

4.2 Thermoplasmonic trapping of silica

In our simulation, we consider three different-sized MNTs and estimated their surface temperature at a fixed intensity of 30 kW/cm^2 . As shown in Fig. 5a, the estimated rise in temperature increases linearly with the size of MNT which is essentially due to increase in number of hotspots. The pronounced heating subsequently results in thermophoretic effects getting enhanced as temperature rises. In the same Fig. 5a, we have plotted thermophoretic interaction radius for three different sizes of MNT, defined as the maximum distance where the thermal gradient is strong enough to attract particles (here, 500 nm silica particle). The thermophoretic effect strongly decreases as the distance between MNT and particle increases. Hence upto a certain distance, thermophoretic force on silica particles can overcome Brownian diffusion, such as to drive the particles close to

the heated MNT surface. Similar observations can be made from Fig. 5b, where the temperature gradient increases in spatial extent as well as in magnitude with respect to MNT size. Here, we have marked (with black arrow) the interaction radius value in the graph for respective MNTs. Interestingly, all of them remains nearly close to a temperature gradient of around $-0.4 \times 10^7 \text{ K/m}$. This value indicates the minimum temperature gradient required to pull 500 nm silica particle with thermophoretic attraction, which is independent of MNT size. The magnitude of the temperature gradient can in principle be related to the Soret coefficient of the 500 nm silica beads, which is unfortunately not available. Experimentally, thermophoretic trapping of a collection of 500 nm silica particles, which is thermophilic i.e. negative Soret coefficient. by a $5 \mu\text{m}$ long MNT is showed in Fig. 6a (also see movie M1), where the colloids can be brought from a distance of around $\sim 7 \mu\text{m}$, by turning the light on and then released by turning the light off. This analysis suggests that it is possible to control the spatial range of thermophoretic attraction by choosing the right combination of geometrical parameters and incident optical power.

To further validate this argument, we have experimentally measured the variation of total trapping force combining plasmonic and thermophoretic contributions for $2 \mu\text{m}$ silica beads using escape velocity measurement technique [14, 37]. We made a microfluidic chamber with an inlet and outlet on a glass slide where the T-MNTs could be held static by laying them down on the surface. A colloidal suspension of silica beads was then injected into the chamber using a syringe pump whose flow rate could be controlled externally. The $2 \mu\text{m}$ silica beads settled down close to the bottom surface of the microfluidic chamber. Once a particle got trapped on the T-MNT surface, the flow velocity was slowly increased until the trapped particles got ejected out of the trap. The laser illumination was kept constant for each measurement. The

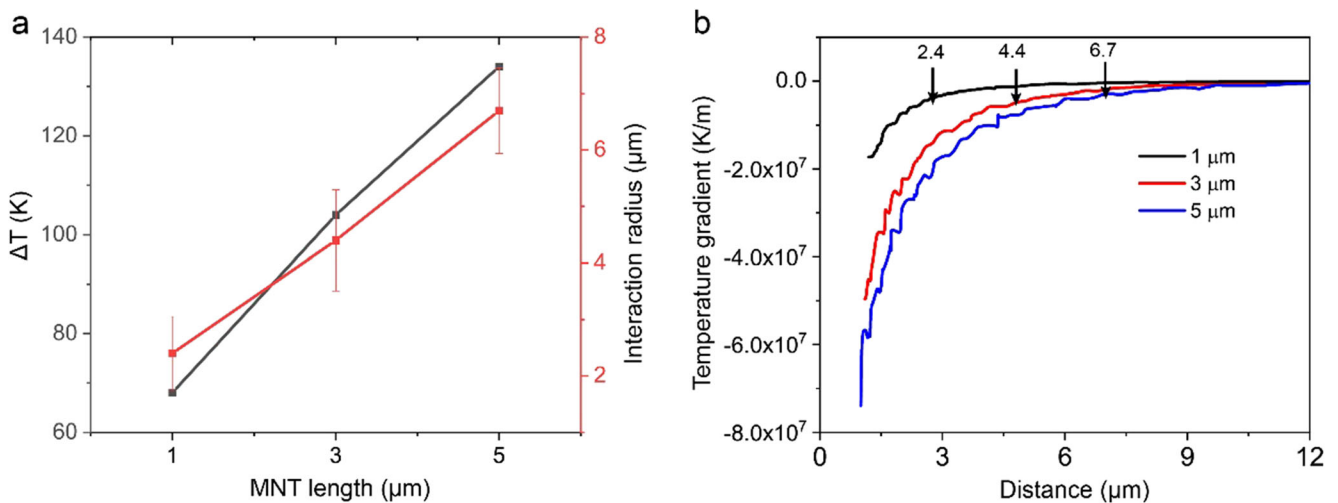


Fig. 5 Temperature evolution in MNTs. **a** Calculated temperature rise and interaction radius (defined later) as a function of MNT length. **b** Calculated temperature gradient plotted as a function of distance from MNT surface for three sizes of MNT. The arrows correspond to positions 2.4, 4.4 and 6.7.

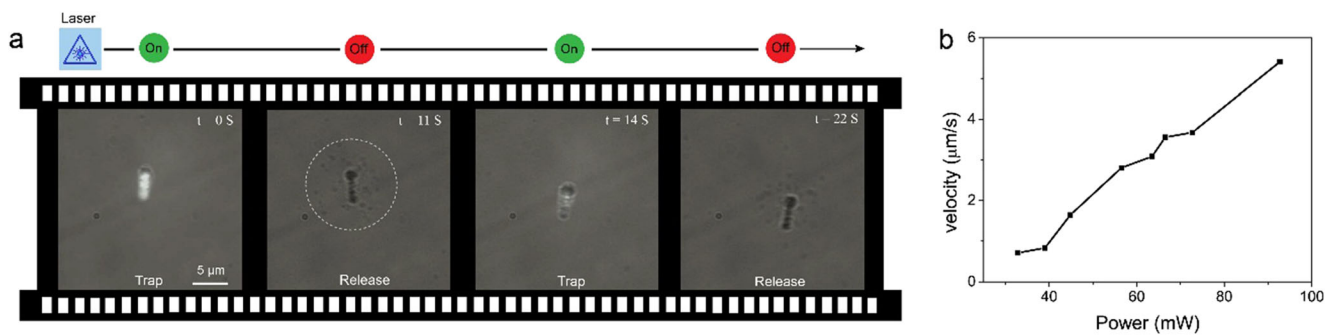


Fig. 6 **a** Thermophoretic trapping of a collection of 500 nm silica particle with 5 μm MNT at 30 kW/cm² light intensity. The untrapped silica beads can be seen as black dots in the frames where the illumination is turned off. **b** Escape velocity of 2 μm silica beads as a function of laser intensity

flow velocity was measured by tracking the motion of a tracer particle which is visible in the same plane as the stuck T-MNT in MATLAB.

At the escape velocity, the effective trapping force is considered to be equal to the viscous drag force described by the modified Stokes law, $F_{tot} = K \cdot 6\pi\eta a v_{esc}$ where η is liquid viscosity, a is the bead radius, v_{esc} is the escape speed of the trapped bead and K is dimensionless correction coefficient, which can depend on the details of the fluid flow profile. The linear scaling of escape velocity with the incident laser power as shown in Fig. 6b indicates a similar trend in increase of total trapping force. This confirms the evolution of enhanced positive thermophoretic effect with increase in T-MNT temperature that aids trapping and as a result increases the speed of operation. This is contrary to what we have seen for polystyrene particles which are thermophobic in nature and therefore could not be trapped by T-MNT at higher optical power levels [19].

Note, the colloids are trapped at the surface of a nanohelix, which is suspended in a fluid and therefore subject to Brownian motion. As a result, there are two modes of position fluctuations: fluctuation of the nanohelix and fluctuation of the nanoparticles trapped on the nanohelix. The mean squared displacement of the nanohelix was measured in a previous experiment from our group and the values of translational diffusion coefficients for a similar geometry was found out to be $\sim 0.5 \mu\text{m}^2\text{s}^{-1}$ which is greater than the nanoparticles

under confinement [38]. We have also observed higher position fluctuation of MNT-bead system in free-space than when it was pinned to a substrate [19]. So, the positioning error ultimately depends only on the fluctuation of the nanohelix itself as observed in previous literature as well [39].

4.3 Non-resonant trapping of polystyrene

In this section, we consider the feasibility of trapping a ‘thermophobic’ (positive Soret coefficient) particle, here PS bead, using the thermoplasmonic MNT, where the key design idea is to reduce the thermal gradient while ensuring the optical gradient forces are high enough to trap the particles. We measured the wavelength dependence of the absorption cross section of the thermoplasmonic MNTs, as shown in Fig. 7a. From the graph, it can be seen that maximum optical absorption happens around 450 nm and reduces significantly beyond 500 nm wavelength. Accordingly, we choose appropriate laser wavelength (here 532 nm) for trapping PS particles where the generated heat is negligible. At this illumination, there is a slight reduction in optical near-field for 532 nm illumination (see Fig. 7b) in comparison to the resonant wavelength of 450 nm.

However, it is still possible to trap PS particles using an off-resonant illumination with reduced heating as shown in a sequence of images in Fig. 8 (also see movie M2). In this case, trapping happens only with electromagnetic gradient forces.

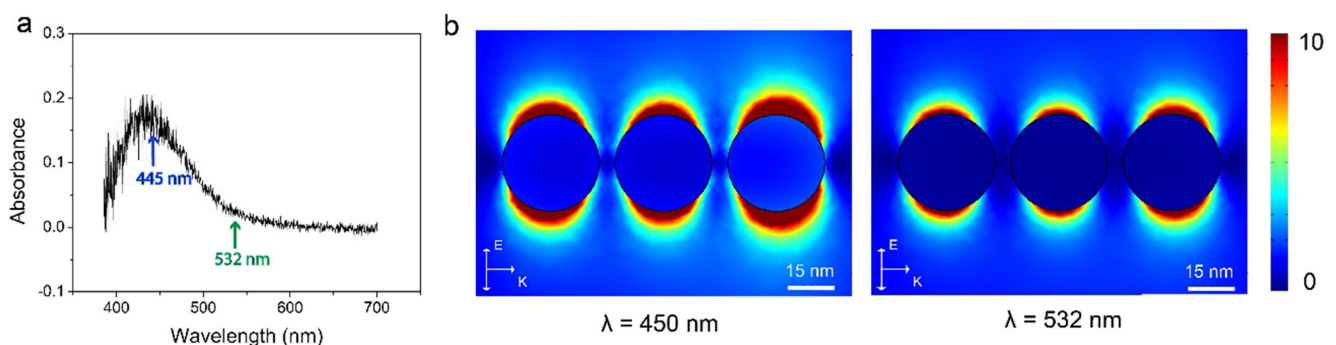


Fig. 7 **a** Optical absorption data for thermoplasmonic MNT peaking around 445 nm wavelength. A laser of wavelength 532 nm is used for off-resonant excitation. **b** Electric field intensity enhancement for 30 nm Ag particles with 450 nm and 532 nm illumination

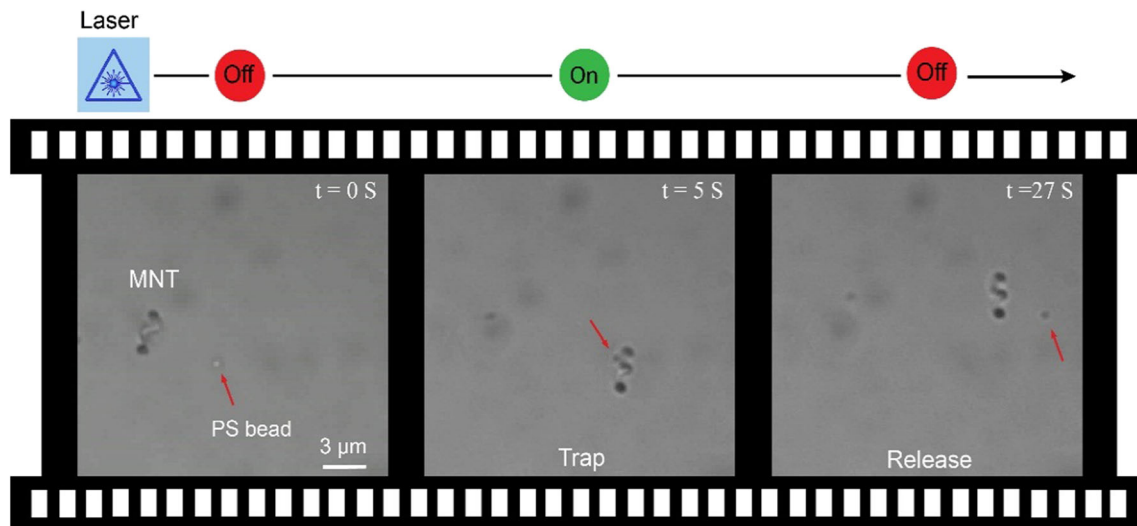


Fig. 8 Trapping of a 1 μm PS bead using a non-resonant illumination of 532 nm wavelength. When the PS bead came close to the T-MNT surface, the laser was switched on which trapped the particle, subsequently the T-

MNT was rotated by applying the magnetic field. The trapped bead rotated synchronously with the helix and was released by turning off the laser

Similar observations have been reported previously with 0.1 μm fluorescent PS beads assembling above Au nanopillars, where stable trapping could be achieved only in a certain window of illumination intensity [40]. Note, the optical absorption was negligibly small at off-resonant illumination (see Fig. 7a), which is why we could not observe any convective flow in these experiments.

5 Conclusion

To summarize, we investigate the temperature rise and associated thermoplasmonic forces near a mobile nanotweezers under optical illumination, combining numerical simulations and experimental investigations. We conclude that it is possible to control the temperature profile and therefore the thermal gradient for a certain illumination power. Accordingly, it is possible to modify thermophoretic forces while keeping the plasmonic gradient forces unchanged. This additional thermal induced force can be useful for trapping materials with negative Soret coefficient. In a similar context, for trapping materials with positive Soret coefficient that do not prefer hot surfaces, it is necessary to suppress the thermal effects which have been achieved here using a non-resonant illumination.

These techniques to controllably tune plasmon induced heating for thermoplasmonic MNTs can aid in designing and developing efficient mobile nanotweezer applications [39, 41]. Although the experiments described here were carried out in deionized water, the nanotweezers are driven by magnetic and optical forces and therefore can be operated in other fluids as well, including various biofluids [42–44]. The demonstrated technology will be useful for on-demand thermophoretic sorting and collective transport. This may also

open the path for plasmofluidic applications such as mixing, sorting, sensing etc. using mobile nanotweezers [45, 46]. The thermoplasmonics MNT may also be employed as mobile nanosources of heat [21] that may be useful for various lab-on-a-chip applications including dynamically controlled bubble generation, photothermal therapy, nanochemistry, molecular transport and many more. In addition, one can envision MNTs to be driven in biological environments such as the intracellular space [43, 47] or cellular surfaces [32, 42], where controlled local sources of heat can trigger biochemical or mechanical (e.g. viscosity [48]) changes on demand.

Acknowledgements S.G thanks Arijit Ghosh, Debayan Dasgupta, Malay Pal, Praneet Prakash and Pranay Mandal for helpful discussions. We thank Department of Biotechnology, India for funding this research. We also acknowledge funding from MHRD, MeitY and DST Nano Mission for supporting the facilities at CeNSE.

References

1. Wang J (2013) Nanomachines: fundamentals and applications. (John Wiley & Sons)
2. Petit T, Zhang L, Peyer KE, Kratochvil BE, Nelson BJ (2012) Selective trapping and manipulation of microscale objects using Mobile microvortices. *Nano Lett* 12:156–160
3. Wang J (2012) Cargo-towing synthetic nanomachines: towards active transport in microchip devices. *Lab Chip* 12:1944
4. Li J, Esteban-Fernández de Ávila, B., Gao W, Zhang L & Wang J (2017) Micro/nanorobots for biomedicine: Delivery, surgery, sensing, and detoxification. *Sci. Robot.* 2, eaam6431
5. Ceylan H, Giltinan J, Kozielski K, Sitti M (2017) Mobile microrobots for bioengineering applications. *Lab Chip* 17:1705–1724

6. Sundararajan S, Lammert PE, Zudans AW, Crespi VH, Sen A (2008) Catalytic Motors for Transport of colloidal cargo. *Nano Lett* 8:1271–1276
7. Burdick J, Laocharoensuk R, Wheat PM, Posner JD, Wang J (2008) Synthetic Nanomotors in microchannel networks: directional microchip motion and controlled manipulation of cargo. *J Am Chem Soc* 130:8164–8165
8. Huang TY, Sakar MS, Mao A, Petruska AJ, Qiu F, Chen XB, Kennedy S, Mooney D, Nelson B (2015) 3D printed microtransporters: compound micromachines for spatiotemporally controlled delivery of therapeutic agents. *Adv Mater* 27:6644–6650
9. Huang T-Y et al (2014) Generating mobile fluidic traps for selective three-dimensional transport of microobjects. *Appl Phys Lett* 105:114102
10. Zhou Q, Petit T, Choi H, Nelson BJ, Zhang L (2017) Dumbbell fluidic tweezers for dynamical trapping and selective transport of microobjects. *Adv Funct Mater* 27:1604571
11. Ashkin A, Dziedzic JM, Bjorkholm JE, Chu S (1986) Observation of a single-beam gradient force optical trap for dielectric particles. *Opt Lett* 11:288
12. Huang TJ et al (2018) Acoustic tweezers for the life sciences. *Nat Methods* 15:1021–1028
13. Righini M, Zelenina A & Quidant R (2007) Parallel and selective trapping in a patterned plasmonic landscape. *Nat Phys.* 61–62. <https://doi.org/10.1109/OMEMS.2007.4373840>
14. Grigorenko AN, Roberts NW, Dickinson MR, Zhang Y (2008) Nanometric optical tweezers based on nanostructured substrates. *Nat Photonics* 2:365–370
15. Juan ML, Gordon R, Pang Y, Eftekhari F, Quidant R (2009) Self-induced back-action optical trapping of dielectric nanoparticles. *Nat Phys* 5:915–919
16. Pang Y, Gordon R (2011) Optical trapping of a single protein. *Nano Lett* 12:6–10
17. Ghosh A, Fischer P (2009) Controlled propulsion of artificial magnetic nanostructured propellers. *Nano Lett* 9:2243–2245
18. Mandal P, Patil G, Kakoty H, Ghosh A (2018) Magnetic active matter based on helical propulsion. *Acc Chem Res* 51:2689–2698
19. Ghosh S, Ghosh A (2018) Mobile nanotweezers for active colloidal manipulation. *Sci Robot* 3:eaq0076
20. Baffou G, Quidant R, García de Abajo FJ (2010) Nanoscale control of optical heating in complex Plasmonic systems. *ACS Nano* 4:709–716
21. Baffou G, Quidant R (2013) Thermo-plasmonics: using metallic nanostructures as nano-sources of heat. *Laser Photon Rev* 7:171–187
22. Piazza R (2004) Thermal forces : colloids in temperature gradients. *J Phys Condens Matter* 16:S4195–S4211
23. Ghosh S, Ghosh A (2018) December. Photothermal effects in mobile nanotweezers. In 2018 4th IEEE International Conference on Emerging Electronics (ICEE) (pp. 1–4). IEEE.
24. Baffou G, Girard C, Quidant R (2010) Mapping heat origin in plasmonic structures. *Phys Rev Lett* 104:1–4
25. Baffou G (2017) *Thermoplasmonics*. (World Scientific)
26. Piazza R, Parola A (2008) Thermophoresis in colloidal suspensions. *J Phys Condens Matter* 20:153102
27. Guyon E (2001) *Physical hydrodynamics*. (Oxford University Press)
28. Dühr S, Braun D (2006) Why molecules move along a temperature gradient. *Proc Natl Acad Sci U S A* 103:19678–19682
29. Braibanti M, Vigolo D, Piazza R (2008) Does thermophoretic mobility depend on particle size? *Phys Rev Lett* 100:1–4
30. Lin L et al (2017) Opto-thermophoretic assembly of colloidal matter. *Sci Adv* 3:e1700458
31. Lin L, Peng X, Mao Z, Wei X, Xie C, Zheng Y (2017) Interfacial-entropy-driven thermophoretic tweezers. *Lab Chip* 17:3061–3070
32. Venugopalan PL, Jain S, Shivashankar S, Ghosh A (2018) Single coating of zinc ferrite renders magnetic nanomotors therapeutic and stable against agglomeration. *Nanoscale* 10:2327–2332
33. Hawkeye MM, Brett MJ (2007) Glancing angle deposition: Fabrication, properties, and applications of micro- and nanostructured thin films. *J Vac Sci Technol A Vacuum, Surfaces, Film* 25:1317
34. Schamel D, Pfeifer M, Gibbs JG, Miksch B, Mark AG, Fischer P (2013) Chiral colloidal molecules and observation of the propeller effect. *J Am Chem Soc* 135:12353–12359
35. Ghosh A, Paria D, Rangarajan G, Ghosh A (2014) Velocity fluctuations in helical propulsion: how small can a propeller be. *J Phys Chem Lett* 5:62–68
36. Baffou G, Berto P, Bermúdez Ureña E, Quidant R, Monneret S, Polleux J, Rigneault H (2013) Photo-induced heating of nanoparticle arrays photo-induced heating of nanoparticle arrays. *ACS Nano* 7:6478–6488
37. Wright WH, Sonek GJ, Berns MW (1994) Parametric study of the forces on microspheres held by optical tweezers. *Appl Opt* 33:1735
38. Dechant A (2019) Estimating the free-space diffusion coefficient of trapped particles. *EPL* 125
39. Ghosh S, Ghosh A (2019) All optical dynamic nanomanipulation with active colloidal tweezers. *Nat Commun* 10:4191
40. Shoji T et al (2013) Reversible photoinduced formation and manipulation of a two-dimensional closely packed assembly of polystyrene nanospheres on a metallic nanostructure. *J Phys Chem C* 117:2500–2506
41. Ghosh A, Ghosh S (2019) Strategies for active colloidal manipulation with plasmonic tweezers (Conference Presentation). in *Optical Trapping and Optical Micromanipulation XVI* (eds. Dholakia, K. & Spalding, G. C.) 11083, 41 (SPIE)
42. Venugopalan PL et al (2014) Conformal Cytocompatible ferrite coatings facilitate the realization of a Nanovoyager in human blood. *Nano Lett* 14:1968–1975
43. Pal M et al (2018) Maneuverability of magnetic Nanomotors inside living cells. *Adv Mater* 30:1800429
44. Roxworthy BJ et al (2014) Plasmonic optical trapping in biologically relevant media. *PLoS One* 9:e93929
45. Wang M, Zhao C, Miao X, Zhao Y, Rufo J, Liu YJ, Huang TJ, Zheng Y (2015) Plasmofluidics: merging light and fluids at the micro-/Nanoscale. *Small* 11:4423–4444
46. Kayani AA, Khoshmanesh K, Ward SA, Mitchell A, Kalantar-zadeh K (2012) Optofluidics incorporating actively controlled micro- and nano-particles. *Biomicrofluidics* 6
47. Yan X et al (2017) Multifunctional biohybrid magnetite microrobots for imaging-guided therapy. *Sci Robot* 2:eaq1155
48. Ghosh A et al (2018) Helical Nanomachines as Mobile viscometers. *Adv Funct Mater* 28:1705687

Publisher's note Springer Nature remains neutral with regard to jurisdictional claims in published maps and institutional affiliations.